

Supporting Information  
for  
Electrically Tunable Transparent Displays for  
Visible Light Based on Dielectric Metasurfaces

Chengjun Zou,<sup>\*,†</sup> Andrei Komar,<sup>‡</sup> Stefan Fasold,<sup>†</sup> Justus Bohn,<sup>†</sup> Alexander A. Muravsky,<sup>¶</sup> Anatoli A. Murauski,<sup>¶</sup> Dragomir N Neshev,<sup>‡</sup> Thomas Pertsch,<sup>†</sup> and  
Isabelle Staude<sup>\*,†</sup>

<sup>†</sup>*Institute of Applied Physics, Abbe Center of Photonics, Friedrich Schiller University Jena,  
07745 Jena, Germany*

<sup>‡</sup>*Nonlinear Physics Centre and Lasser Physics Centre, Research School of Physics and  
Engineering, The Australian National University, Canberra, 2601 ACT Australia*

<sup>¶</sup>*Institute of Chemistry of New Materials, National Academy of Science of Belarus,  
220141, Minsk, Belarus*

E-mail: chengjun.zou@uni-jena.de; isabelle.staude@uni-jena.de

## S1. Alignment Quality

In order to quantify how the alignment quality (AQ) of the LCs is influenced by applying the photoalignment layer on both the upper electrode and the metasurface instead of on the upper electrode only, we conducted alignment quality measurements of assembled LC cells using the setup shown in Figure S1(a). A He-Ne laser (633 nm wavelength) is used as light source. The laser beam passes the LC cell, which is sandwiched between two linear polarizers  $p1$  and  $p2$ . In a first measurement, the polarization axes of both polarizers are oriented along the LC prealignment direction. The transmitted intensity  $I_1$  is recorded using a power meter. In a second measurement, the polarizer  $p2$  is rotated by  $90^\circ$ , and the transmitted intensity  $I_2$  is recorded. The alignment quality is calculated as  $AQ = (I_1 - I_2)/(I_1 + I_2)$ . A value over 0.9 is generally regarded as a good LC alignment in the LC display industry. Using this method, we measured the AQ of two independently assembled metasurface LC cells which both used the same metasurface sample as the bottom electrode. For the first LC cell, we coated both the metasurface and the upper electrode with a 15 nm thick AtA-2 layer, while for the second cell, we coated only the upper electrode. Details of the coating process are described in the *Methods*. The measured AQ at the center of the metasurface reaches 0.97 and 0.84 for the first and the second cell, respectively, indicating a clear improvement of the alignment quality achieved in the the LC metasurface cell if both electrodes are coated. Note that the anchoring energy of exposed AtA-2 itself is comparable with that

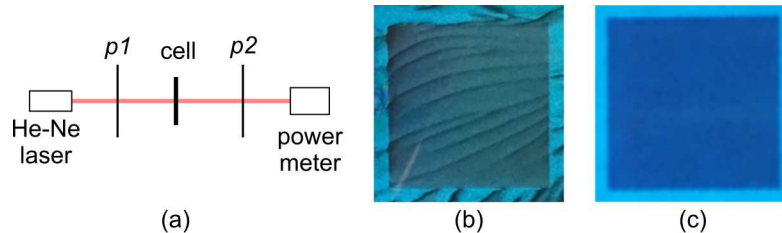


Figure S1: (a) Schematic of the measurement setup used for quantitative evaluation of the alignment quality of LC metasurface cells. (b,c) Photograph of a back-illuminated LC metasurface cell observed through two parallel linear polarizers. In (b), only the upper electrode is coated with AtA-2, in (c) both the metasurface and the upper electrode are coated with AtA-2.

of mechanically brushed Nylon-6,<sup>1</sup> a common alignment material used in previous works.<sup>2,3</sup> Furthermore, to visually assess the spatial homogeneity of the LC prealignment inside the LC metasurface cell, we again placed the cell between two parallel polarizers oriented along the LC prealignment direction and back-illuminated it with a blue area light. Photographs of the  $5 \times 5 \text{ mm}^2$  large metasurface integrated into the two assembled LC cells in the described configuration are shown in Fig. S1(b,c). The cell with only a single AtA-2 layer is shown in Fig. S1(b). The clearly observed dark stripes are indicative of the formation of LC domains and poor homogeneity of the alignment over large areas. In contrast, for the LC cell with two AtA-2 layers shown in Fig. S1(c), an excellent spatial homogeneity is observed. Our results illustrate that by using the photoalignment technique, which allows us to coat the alignment layer not only onto the upper electrode but also onto the metasurface sample, we improve both the quality and spatial homogeneity of the LC alignment accuracy. We believe this to be a critical advance for real-world applications of LC-integrated metasurfaces.

## S2. Calculation of the Voltage-Dependent LC Director Orientation

The voltage-dependent orientation of the director of the nematic LC E7 was calculated based on the simplified LC cell structure illustrated in Fig. S2(a). The alignment layers

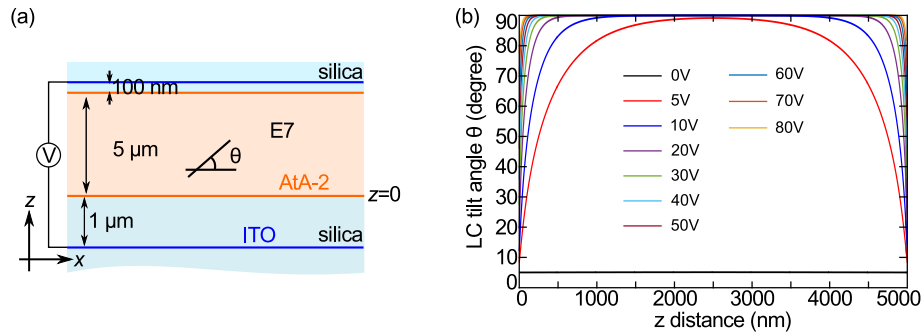


Figure S2: Calculation of voltage-dependent spatial distribution of LC tilt angles. (a) Model considered for the calculation. (b) Calculated LC tilt angle distribution for a  $5 \mu\text{m}$  LC cell with an applied 1 kHz AC root-mean-square voltage from 0 to 80V.

provide defined anchoring conditions for the LC director at the alignment layer surface, which determine the prealignment direction (here:  $x$ -direction). Deviations from the perfect prealignment direction, e.g. induced by application of an external voltage, are characterized by two angles, the in-plane deviation angle  $\varphi(x, y, z)$  and the out-of-plane deviation angle  $\theta(x, y, z)$ . Both angles can have a spatial dependence depending on the specifics of the model or experimental situation. In our model, the external voltage only affects the out-of-plane angle  $\theta(x, y, z)$ , such that the in-plane deviation angle  $\varphi(x, y, z)$  is always zero. Furthermore, due to the symmetry of the considered model, the out-of-plane angle will only depend on the  $z$ -coordinate, i.e.  $\theta(z)$ . Initially, without any applied voltage,  $\theta(z)$  is zero at the surface, i.e.  $\theta(0) = 0^\circ$ . However, when a finite voltage is applied to the cell, as shown in Fig S2(a), the E7 molecules, due to their dipolar characteristics, tend to re-orient along the electric field lines, which are oriented perpendicular to the  $x - y$  substrate plane in our case. Inside the cell, the dependence of the LC director orientation on the  $z$ -coordinate is determined by the balance of the electric field energy, the bulk energy of LC elastic deformation, and the surface energy  $A_\theta$ . The latter is related to the finite polar anchoring energy  $W_\theta$  of the specific alignment material. The Rapini-Papoular surface energy for polar and azimuthal contributions is given by:  $A_\theta = W_\theta \sin^2(\theta - \theta_0)$  and  $A_\varphi = W_\varphi \sin^2(\varphi - \varphi_0)$ ,<sup>4</sup> respectively.

The polar anchoring coefficient for the AtA-2 alignment material is  $W_\theta = 1 \times 10^{-3} \text{ J/m}^2$ .<sup>5</sup> The LC director orientation  $\theta(z)$  was calculated using a previously developed the real-time simulation software for electro-optical calculations of LC cells<sup>6</sup> for an applied 1 kHz AC root mean square (RMS) voltage ranging from 0 to 80V. The calculated results are presented in Fig. S2(b). In particular, the simulations predict  $\theta(0) = 19.6^\circ$  at the alignment layer surface for an applied voltage of 20V.  $\theta(0)$  increases to  $77.4^\circ$  at 80V. Meanwhile, at the center of the LC cell  $\theta(z = 2.5 \mu\text{m})$  reaches  $90^\circ$  in both cases. Note, however, that the orientation of the LC molecules near the alignment layer surface plays the dominant role in the electrical tuning of the metasurface transmittance, since the optical near-fields are strongest in this region.

## S3. Numerical Calculations

### S3.1 Electromagnetic Modeling of the LC Metasurface Cell

In order to design the metasurface sample and to compare our experimental results with theoretical calculations, we perform numerical simulations using the commercial software package CST Microwave Studio. To implement the LC as an anisotropic and spatially varying material, we discretize the  $z$ -dependence of the LC director orientation and model the LC as a multilayer stack. The orientation of the LC anisotropy axis in each layer is determined from the previously calculated  $\theta(z)$  distribution (see Section S2). The pink layers shown in the zoom image is the AtA-2 layer with a thickness of 15 nm. The photoalignment layer AtA-2 is modeled as a uniaxial anisotropic dielectric material with its refractive index of  $n_{\parallel} = 2$  and  $n_{\perp} = 1.5$  in the considered wavelength range. The top of the metasurface is defined as the  $z = 0$  position, such that the  $z = 0$  positions in Fig. S3 and Fig. S2 coincide. Furthermore, the LC material located in the negative  $z$  region in Fig. S3 is modeled with the same properties as the LC layer at  $z = 0$ .

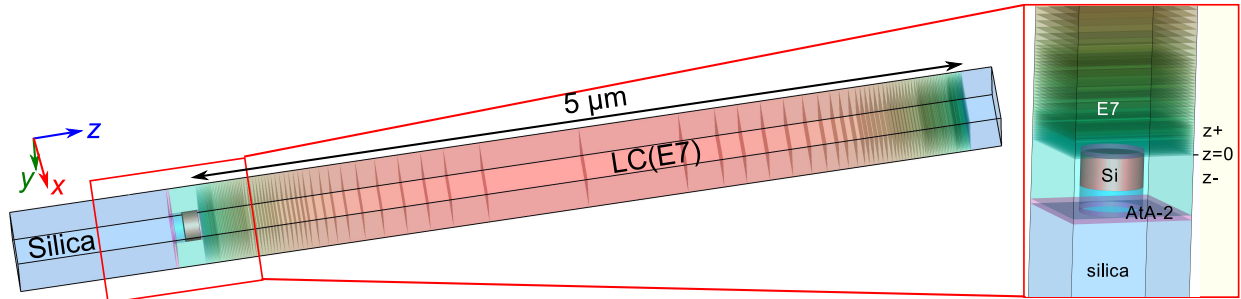


Figure S3: Sketch of the model used to calculate voltage-dependent transmittance spectra of the LC metasurface cell for the case of  $V_{\text{RMS}} = 5V$ : The LC inside the cell is modeled as a multilayer stack, where the orientation of the LC anisotropy axis is a function of the layer number.

### S3.2 Near-field profiles of the uninfiltrated metasurfaces

Figure S4 shows the simulated normalized electric fields for the two resonance dips appearing in the transmittance spectrum of the bare metasurface before LC-infiltration under the  $y$ -polarized normally incident plane wave excitation (see Fig. 1(c)). The near-field characteristics allow us to identify the resonance modes at 625 nm and 653 nm as the electric dipole and magnetic dipole modes of the nanocylinders, respectively.

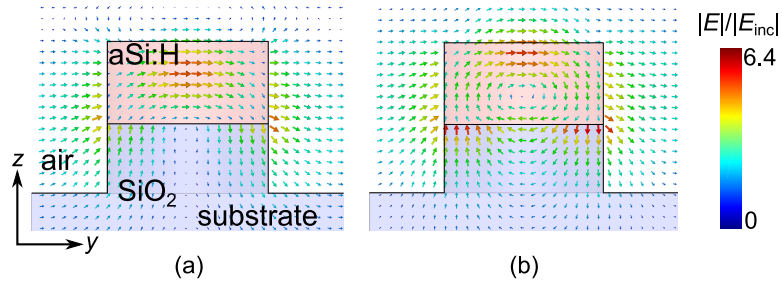


Figure S4: Simulated normalized electric field distributions. (a) Electric dipole resonance at 625 nm. (b) Magnetic dipole resonance at 653 nm.

### S3.3 Near-field profile of the LC-infiltrated metasurfaces

Figure S5 shows the simulated normalized electric fields for the resonance dips at 681 nm and 704 nm, which are present in the transmittance spectrum of the LC-infiltrated metasurface for linearly-polarized incidence along the prealignment direction at  $V_{\text{rms}} = 0\text{V}$  (see Fig. 3(a)). From the electric-field distribution, we can conclude that the resonances at 681 nm and 704 nm correspond to magnetic and electric dipole mode of the nanocylinders, respectively.

Apart from the electric and magnetic dipolar resonances, an additional resonance is observed both in the simulated and in the measured transmittance spectra, when the incident light is linearly polarized along the LC prealignment direction. The simulated near fields of this mode for applied voltages of 0V, 30V, and 60V are shown in Fig. S6. It can be seen that an electric dipole mode with a dominant out-of-plane component is excited in the nanocylinders. Out-of-plane dipole modes cannot usually couple to the far-field at normal incidence due to the emission characteristics of a dipole, which does not emit along its axis.

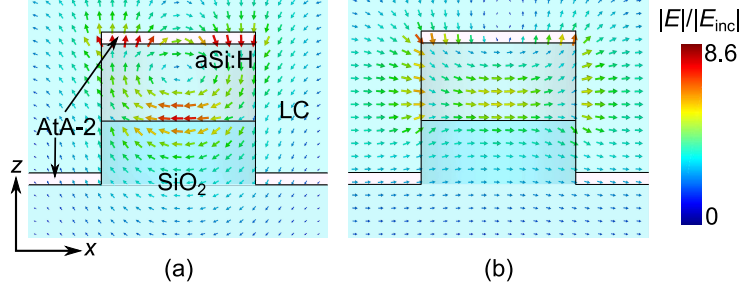


Figure S5: Simulated normalized electric fields. (a) Magnetic dipole resonance at 681 nm. (b) Electric dipole resonance at 704 nm.

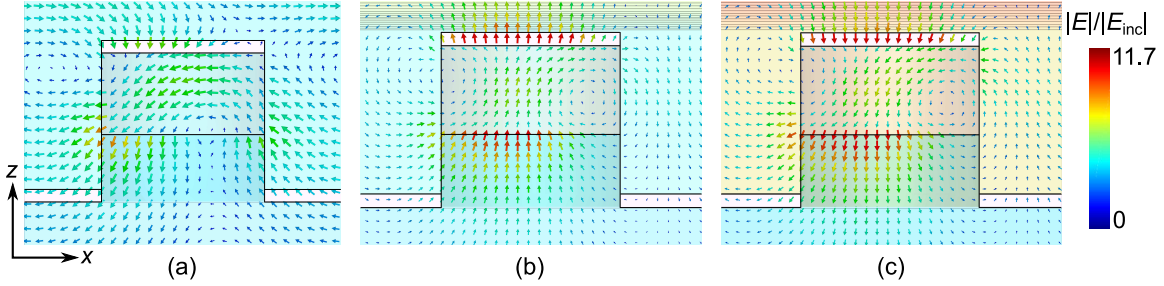


Figure S6: Simulated normalized electric-field profiles of the dark mode supported by the LC-infiltrated dielectric metasurface. (a) 0V,  $\lambda = 651$  nm. (b) 30V,  $\lambda = 662$  nm. (c) 60V,  $\lambda = 672$  nm.

They are therefore often called dark resonances. In our case the normally incident light can couple to this otherwise dark mode due to the symmetry break induced by the anisotropic LC refractive index.

## S4. Switchable Display Imaging Setup

**Switchable display imaging** The voltage-dependent spatially resolved transmission of the tunable metasurface display is imaged with a custom-built Köhler illumination setup. A sketch of the setup is shown in Fig. S7. A halogen lamp is used as a light source. Its emission is focused by a 2-inch condenser lens onto a  $\sim 500$   $\mu\text{m}$  diameter iris. The light transmitted through the iris is subsequently collimated by a  $f = 75$  mm convex lens and directed onto a tunable filter (HSi300 HyperSpectral Imaging System, Gooch & Housego) set to a center wavelength of 669 nm and a bandwidth of 2.3 nm. The filtered light is linearly polarized. A

dedicated lens system in front of the metasurface LC cell is used to collimate the light and ensure homogeneous illumination of the metasurface sample. The red dashed light denotes the imaging optical path, while the blue dashed light denotes the conjugated optical path. A  $f = 150$  mm lens is selected in order to obtain a weakly focused 5 mm focal spot that covers the entire metasurface area. Two additional lenses are used to image the sample on the chip of a CCD camera. To record the images shown in Fig. 5(b), an AC voltage was applied to the metasurface LC cell and tuned from 0 to 20V 5V steps.

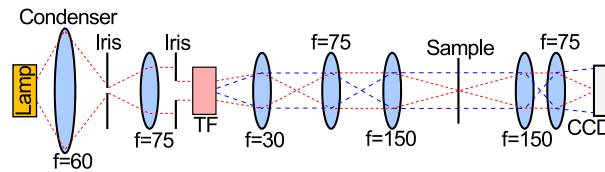


Figure S7: Sketch of the custom-built Köhler illumination imaging setup. TF stands for the tunable filter for incident wavelength selection.

## References

- (1) Wnek, M.; Moscicki, J.; d’Alessandro, A.; Campoli, F.; Maltese, P.; Buivydas, M.; Matuszczyk, M.; Matuszczyk, T.; Lagerwall, S. T. Anchoring Conditions for Different Aligning Materials from Dielectric Behavior of SSFLC Cells. *Liquid Crystals: Physics, Technology, and Applications*. 1998; pp 86–90.
- (2) Komar, A.; Fang, Z.; Bohn, J.; Sautter, J.; Decker, M.; Miroshnichenko, A.; Pertsch, T.; Brener, I.; Kivshar, Y. S.; Staude, I.; Neshev, D. N. Electrically Tunable All-Dielectric Optical Metasurfaces Based on Liquid Crystals. *Appl. Phys. Lett.* **2017**, *110*, 071109.
- (3) Bohn, J.; Bucher, T.; Chong, K. E.; Komar, A.; Choi, D.-Y.; Neshev, D. N.; Kivshar, Y. S.; Pertsch, T.; Staude, I. Active Tuning of Spontaneous Emission by Mie-resonant Dielectric Metasurfaces. *Nano Lett.* **2018**, *18*, 3461–3465.

- (4) Faetti, S. Azimuthal Anchoring Energy of A Nematic Liquid Crystal at A Grooved Interface. *Phys. Rev. A* **1987**, *36*, 408.
- (5) Muravsky, A. *Next Generation of Photoalignment: Reversible Intermolecular Bonds*; Saarbrücken, Germany, VDM Verlag Dr. Müller, 2009.
- (6) Murauski, A.; Serdechnaya, S.; Kwok, H.-S. P-132: Real-Time Simulation Software for Electro-Optical Calculation of LC Cells. SID Int. Symp. Dig. Tech. Pap. 2007; pp 702–705.